Available online at www.sciencedirect.com
SCIENCE DIRECT
Journal of Solid State Chemistry 179 (2006) 1750–1756
JOURNAL OF SOLID STATE CHEMISTRY
www.elsevier.com/locate/jssc

Synthesis, structural characterization, and magnetic properties of the antiferromagnetic double perovskites Ln_2LiOsO_6 (Ln = La, Pr, Nd, Sm)

William R. Gemmill, Mark D. Smith, Hans-Conrad zur Loye*

Department of Chemistry and Biochemistry, University of South Carolina, Columbia, SC 29208, USA

Received 30 January 2006; received in revised form 1 March 2006; accepted 10 March 2006
Available online 18 March 2006

Abstract

A series of osmium double perovskite oxides, Ln_2LiOsO_6 (Ln = La, Pr, Nd, Sm), has been prepared as single crystals from acidic molten hydroxide. All four oxides crystallize in the monoclinic space group $P2_1/n$ (Glazer tilt system #10, $a^-a^-b^+$), forming a 1:1 ordered rock salt lattice of Li^+ and Os^{5+} cations. Magnetic susceptibility measurements show that these compounds are antiferromagnetic at low temperature with ordering temperatures of 39, 35, 23, and 32 K for Ln_2LiOsO_6 (Ln = La, Pr, Nd, Sm), respectively.

Keywords: Crystal growth; Osmium oxides; Magnetic properties; La_2LiOsO_6; Pr_2LiOsO_6; Nd_2LiOsO_6; Sm_2LiOsO_6

1. Introduction

Perovskite oxides are perhaps the most studied family of compounds in solid-state chemistry due to their inherent ability to accommodate a wide range of elemental compositions and to display a wealth of structural variations. Perovskites have the general formula ABO_3, where A typically represents a large electropositive cation and B represents a smaller transition metal or main group ion. In its ideal form, the cubic ABO_3 perovskite can be described as consisting of corner sharing BO_6 octahedra with the A cation occupying the 12-fold coordination site in the center of 8 such octahedra. The structure can also be described as resulting from the stacking of close packed [AO_3] layers in a cubic (abc) fashion followed by the filling of the generated octahedral sites by the B cations. The ideal double perovskite structure of the general formula $A_2BB'O_6$ is obtained when the B cation is substituted by a B' cation in an ordered 1:1 fashion, doubling the unit cell.

Recently, we have been interested in the single-crystal growth of double perovskites of the general composition $Ln_2BB'O_6$, where Ln signifies a trivalent lanthanide metal, B is a monovalent alkali metal, and B' represents a pentavalent platinum group metal. To prepare these phases, we have successfully developed an effective method of single-crystal growth employing molten hydroxides [1–5]. The acid–base chemistry of hydroxide fluxes, described by the Lux–Flood acid–base definition [6,7] allows for a wide range of species to be present in solution, an essential prerequisite for their incorporation into single crystals. Also, it has been shown that molten hydroxides are capable to dissolve the metals of the lanthanide series [8,9], where the solubility of the lanthanides is dictated by the acid–base properties of the melt. Specifically, the water content of the melt must be controlled to enable the dissolution of the lanthanide oxides (Ln_2O_3's), which are only soluble in acidic "wet" melts [6–8,10].

Interestingly, there has been a significant amount of recent work carried out on the preparation of new perovskite and complex oxide phases containing osmium owing, at least in part, to the discovery of superconductivity in KOs_2O_6 (T_c = 9.6 K) [11] and $RbOs_2O_6$ (T_c = 6.3 K) [12]. Other interesting properties have been found in complex osmium oxides including a metal–insulator transition (225 K) in $Cd_2Os_2O_7$ [13,14] and spin–flop transitions in both Pr_2NaOsO_6 and Nd_2NaOsO_6 [2]. Recent reports of osmium containing oxides also include $Ba_{11}Os_4O_{24}$ [15], Li_7OsO_6 [16], and K_2OsO_5 [17]. To a rather short list of reported oxides of osmium we have

*Corresponding author. Fax: +1 803 777 8508.
E-mail address: jssc@mail.chem.sc.edu (H.-C. zur Loye).

0022-4596/$ - see front matter © 2006 Elsevier Inc. All rights reserved.
doi:10.1016/j.jssc.2006.03.010

contributed Ba_2MOsO_6 (M = Li, Na) [18], $Ba_3MOs_2O_9$ (M = Li, Na) [19], Ln_3OsO_7 (Ln = Sm, Eu, Gd) [20], Ln_2NaOsO_6 (Ln = La, Pr, Nd) [2], and most recently A_2NiOsO_6 (A = Sr, Ca) [21]. In an extension of this work we prepared the series of double perovskites, Ln_2LiOsO_6 (Ln = La, Pr, Nd, Sm). The powder preparation and magnetic susceptibility of La_2LiOsO_6 has been previously reported [22]. The single-crystal growth, structural characterization, and magnetic properties of the four title compounds are reported herein.

2. Experimental

2.1. Crystal growth

For all compounds, 1.00 mmol Os (J&J Materials), 1.00 mmol Ln_2O_3 (Alfa Aesar, REaction, 99.9%), 1.0 g $LiOH \cdot H_2O$ (Alfa Aesar, 98%), 3.0 g KOH (Fisher, ACS reagent), and 1.0 g H_2O were placed into silver tubes (10 cm long, 1.25 cm diameter) that had been flame sealed on one end. The silver tubes were then crimped shut on the other end and placed into a box furnace. Optimizing the reaction conditions to obtain the highest quality single crystals yielded the following reaction conditions: for La_2LiOsO_6 the reaction was carried out at 625 °C for 24 h after which the furnace was shut off. For Pr_2LiOsO_6 the reaction was carried out at 600 °C for 12 h followed by cooling to 400 °C at 1 °C/min and finally shutting off the furnace. For both Nd_2LiOsO_6 and Sm_2LiOsO_6 the reactions were heated at 600 °C for 24 h and subsequently cooled by turning off the furnace. The flux in all cases was dissolved with methanol (ACS reagent, used as received) (the lithium containing crystals are somewhat water sensitive and, hence, water should not be used to dissolve the flux), aided by the use of sonication, followed by manual isolation of the crystals.

2.2. Single-crystal X-ray diffraction

For the structure determination of La_2LiOsO_6 an irregular black crystal fragment chipped from a multicrystalline aggregate was used, and for Ln_2LiOsO_6 (Ln = Pr, Nd, Sm) black block-like crystals were used and mounted onto the end of thin glass fibers. X-ray intensity data were measured at 294 K for La_2LiOsO_6, Nd_2LiOsO_6, and Sm_2LiOsO_6 and at 150 K for Pr_2LiOsO_6 on a Bruker SMART APEX diffractometer (Mo$K\alpha$ radiation, $\lambda = 0.71073$ Å) [23]. The data collection covered 100.0% of reciprocal space to $2\theta = 70.2°$ (average redundancy = 5.42) for La_2LiOsO_6, 99.8% of reciprocal space to $2\theta = 70.56°$ (average redundancy = 5.0) for Pr_2LiOsO_6, 99.4% of reciprocal space to $2\theta = 70.1°$ (average redundancy = 4.0) for Nd_2LiOsO_6, and 98.8% of reciprocal space to $2\theta = 65.3°$ (average redundancy = 3.2) for Sm_2LiOsO_6. Raw area detector data frame integration and Lp corrections were carried out with SAINT+ [23]. Final unit cell parameters were determined by least-squares refinement of all reflections with $I > 5\sigma(I)$ from each data set (2855 for La_2LiOsO_6, 2582 for Pr_2LiOsO_6, 3661 for Nd_2LiOsO_6, and 3173 for Sm_2LiOsO_6). Analysis of each data set showed negligible crystal decay during data collection. An empirical absorption correction was applied with SADABS [23].

The compounds Ln_2LiOsO_6 (Ln = Pr, Nd, Sm) crystallize with monoclinic symmetry in the space group $P2_1/n$ as determined by the pattern of systematic absences in the intensity data. This structural model was refined by full-matrix least-squares against F^2, with SHELXTL [24].

Table 1
Crystal data and structural refinement for Ln_2LiOsO_6 (Ln = La, Pr, Nd, Sm)

Empirical formula	La_2LiOsO_6	Pr_2LiOsO_6	Nd_2LiOsO_6	Sm_2LiOsO_6
Formula weight (g/mol)	570.96	574.96	581.62	593.84
Space group	$P2_1/n$	$P2_1/n$	$P2_1/n$	$P2_1/n$
Temperature (K)	294(2)	150(1)	294(2)	294(2)
Unit-cell dimensions				
a (Å)	5.5603(2)	5.4611(2)	5.4345(2)	5.3836(2)
b (Å)	5.6564(2)	5.7179(2)	5.7383(2)	5.7419(2)
c (Å)	7.8662(3)	7.7328(3)	7.7193(3)	7.6510(3)
β (deg)	90.147(1)	90.407(2)	90.496(1)	90.688(1)
V (Å^3)	247.401(14)	241.881(15)	240.716(15)	236.491(15)
Z	2	2	2	2
Density (calculated) (Mg/m^3)	7.664	7.894	8.024	8.339
Absorption coefficient (mm^{-1})	42.520	45.971	47.523	51.247
Reflections collected	6431	5931	4141	3837
Independent reflections	1092 ($R_{int} = 0.0356$)	1083 ($R_{int} = 0.0381$)	1080 ($R_{int} = 0.0254$)	853 ($R_{int} = 0.0266$)
Goodness-of-fit on F^2	1.103	1.065	1.204	1.096
Final R indices	$R_1 = 0.0251$	$R_1 = 0.0255$	$R_1 = 0.0218$	$R_1 = 0.0229$
$[I > 2\sigma(I)]$	w$R_2 = 0.0513$	w$R_2 = 0.0522$	w$R_2 = 0.0488$	w$R_2 = 0.0551$
R indices (all data)	$R_1 = 0.0294$	$R_1 = 0.0295$	$R_1 = 0.0234$	$R_1 = 0.0239$
	w$R_2 = 0.0530$	w$R_2 = 0.0538$	w$R_2 = 0.0493$	w$R_2 = 0.0556$
Residual electron density (e$^-$/Å^3)	2.725 and −2.525	2.147 and −2.964	2.079 and −2.232	2.187 and −1.520

All atoms were refined with anisotropic displacement parameters, except for the Li atom (in all four compounds), which was refined isotropically. Refinement of the site occupation factors for the heavy metal atoms showed no significant deviation from unity occupancy.

Due to the monoclinic beta angles of 90.147(1)°, 90.407(2)°, 90.496(1)°, and 90.688(1)° for La_2LiOsO_6, Pr_2LiOsO_6, Nd_2LiOsO_6, and Sm_2LiOsO_6, respectively, a check for pseudo-orthorhombic twinning was performed by including the twin matrix $\{100/0\bar{1}0/00\bar{1}\}$ in a refinement cycle. The refined twin fractions (SHELX BASF parameter) were 1.00/0.0 in each case, indicating genuine single crystals for all four compounds. The twin matrix was not included in the final cycles. Relevant crystallographic data from the single-crystal structure refinements for the compounds Ln_2LiOsO_6 (Ln = La, Pr, Nd, Sm) are compiled in Table 1. For all four compounds, atomic positions are selected interatomic distances and angles are summarized in Tables 2 and 3, respectively.

2.3. Scanning electron microscopy

Environmental scanning electron micrographs (ESEM) of several single crystals were obtained using a FEI Quanta 200 ESEM instrument utilized in the low vacuum mode. ESEM images of representative crystals of Nd_2LiOsO_6 and Sm_2LiOsO_6 are shown in Figs. 1a and b, respectively. The crystal morphology is similar to that of other related double perovskites, namely Ln_2NaMO_6 (Ln = La, Pr, Nd, Sm [4], M = Ru [3], Os [2], Ir [1]) and Ln_2LiIrO_6 (Ln = La, Pr, Nd, Sm, Eu) [5]. Energy dispersive spectroscopy (EDS) verified the presence of the rare earth element (lanthanum, praseodymium, neodymium, or samarium), osmium, and oxygen for Ln_2LiOsO_6 (Ln = La, Pr, Nd, Sm). Furthermore, within the detection limit of the instrument, no other extraneous elements were detected.

Table 2
Atomic coordinates and equivalent displacement parameters for La_2LiOsO_6, Pr_2LiOsO_6, Nd_2LiOsO_6, and Sm_2LiOsO_6

	x	y	z	U_{eq}
La_2LiOsO_6				
La (4*e*)	0.4912(1)	0.0460(1)	0.2511(1)	0.009(1)
Li (2*a*)	0	0	0	0.016(3)[a]
Os (2*b*)	1/2	1/2	0	0.007(1)
O(1) (4*e*)	0.2182(7)	0.3011(7)	0.0415(5)	0.009(1)
O(2) (4*e*)	0.5788(7)	0.4828(7)	0.2418(5)	0.009(1)
O(3) (4*e*)	0.3032(7)	0.7818(7)	0.0437(5)	0.010(1)
Pr_2LiOsO_6				
Pr (4*e*)	0.4864(1)	0.0626(1)	0.2512(1)	0.005(1)
Li (2*a*)	0	0	0	0.008(3)[a]
Os (2*b*)	1/2	1/2	0	0.005(1)
O(1) (4*e*)	0.2064(7)	0.3114(7)	0.0456(5)	0.007(1)
O(2) (4*e*)	0.5920(8)	0.4712(7)	0.2439(6)	0.008(1)
O(3) (4*e*)	0.3163(7)	0.7868(7)	0.0504(6)	0.007(1)
Nd_2LiOsO_6				
Nd (4*e*)	0.4853(1)	0.0657(1)	0.2511(1)	0.005(1)
Li (2*a*)	0	0	0	0.010(3)[a]
Os (2*b*)	1/2	1/2	0	0.003(1)
O(1) (4*e*)	0.2050(6)	0.3149(6)	0.0463(4)	0.006(1)
O(2) (4*e*)	0.5947(7)	0.4701(7)	0.2441(5)	0.006(1)
O(3) (4*e*)	0.3189(7)	0.7873(7)	0.0516(5)	0.007(1)
Sm_2LiOsO_6				
Sm (4*e*)	0.4832(1)	0.0710(1)	0.2513(1)	0.005(1)
Li (2*a*)	0	0	0	0.008(3)[a]
Os (2*b*)	1/2	1/2	0	0.004(1)
O(1) (4*e*)	0.2009(8)	0.3173(8)	0.0492(6)	0.006(1)
O(2) (4*e*)	0.6026(9)	0.4656(8)	0.2449(6)	0.006(1)
O(3) (4*e*)	0.3237(9)	0.7895(9)	0.0548(6)	0.008(1)

[a]Refined isotropically.

Table 3
Selected interatomic distances (Å), bond angles (deg) for La_2LiOsO_6, Pr_2LiOsO_6, Nd_2LiOsO_6, and Sm_2LiOsO_6

	La_2LiOsO_6	Pr_2LiOsO_6	Nd_2LiOsO_6	Sm_2LiOsO_6
Ln–O(1)	2.438(4)	2.382(4)	2.370(4)	2.339(5)
	2.663(4)	2.619(4)	2.612(4)	2.578(5)
	2.747(4)	2.666(4)	2.654(4)	2.629(5)
Ln–O(2)	2.418(4)	2.361(4)	2.348(4)	2.310(5)
	2.520(4)	2.411(4)	2.396(4)	2.356(5)
Ln–O(3)	2.445(4)	2.398(4)	2.391(4)	2.362(5)
	2.660(4)	2.602(4)	2.591(4)	2.562(5)
	2.766(4)	2.716(4)	2.711(4)	2.696(5)
Li–O(1) (× 2)	2.116(4)	2.138(4)	2.154(4)	2.149(5)
Li–O(2) (× 2)	2.081(4)	2.053(5)	2.053(4)	2.044(5)
Li–O(3) (× 2)	2.117(4)	2.149(4)	2.154(4)	2.158(5)
Os–O(1) (× 2)	1.957(4)	1.967(4)	1.959(3)	1.962(4)
Os–O(2) (× 2)	1.953(4)	1.956(5)	1.957(4)	1.957(5)
Os–O(3) (× 2)	1.964(4)	1.965(4)	1.963(4)	1.962(5)
Os–O(1)–Li	153.6(2)	149.1(2)	148.07(19)	146.3(2)
Os–O(2)–Li	154.3(2)	149.4(2)	148.6(2)	145.9(3)
Os–O(3)–Li	152.7(2)	148.2(2)	147.4(2)	145.5(3)

2.4. Magnetic susceptibility

The magnetic susceptibility of the compounds Ln_2LiOsO_6 (Ln = La, Pr, Nd, Sm) was measured using a Quantum Design MPMS XL SQUID magnetometer. For the magnetic measurements, loose crystals of Ln_2LiOsO_6 (Ln = La, Pr, Nd, Sm) were placed into gelatin capsules, which were placed inside plastic straws. Samples were measured under both zero-field-cooled (ZFC) and field-cooled (FC) conditions. For all measurements, the magnetization was measured in the temperature range of 2–300 K. Susceptibility measurements were carried out in an applied field of 10 kG. The very small diamagnetic contribution of the gelatin capsule containing the sample had a negligible contribution to the overall magnetization, which was dominated by the sample signal.

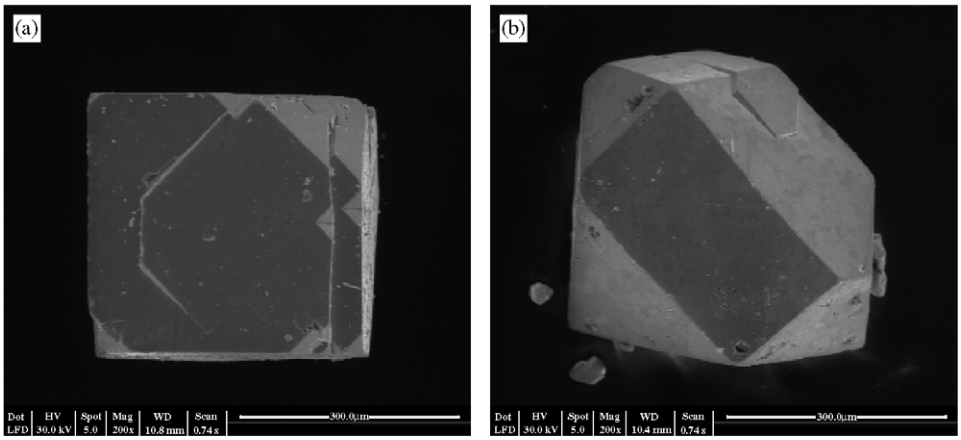

Fig. 1. ESEM images of flux grown crystals of (a) Nd_2LiOsO_6 and (b) Sm_2LiOsO_6. Both crystals measure approximately 300 μm on edge.

3. Results and discussion

3.1. Crystal structure

Small black crystals of Ln_2LiOsO_6 (Ln = La, Pr, Nd, Sm) were grown from molten hydroxide fluxes in which the flux acted as both a solvent and a reactant. ESEM images of representative crystals of Nd_2LiOsO_6 and Sm_2LiOsO_6 are shown in Figs. 1a and b, respectively.

The title compounds Ln_2LiOsO_6 (Ln = La, Pr, Nd, Sm) crystallize in the space group $P2_1/n$, with the monoclinic-distorted structure type, general formula $A_2BB'O_6$, Fig. 2. This space group allows for the 1:1 ordered arrangement of the B and B' cations in a rock-salt type lattice and the tilting of the BO_6 and $B'O_6$ octahedra to accommodate the small size of the A cation. The Glazer tilt system assigned to the $P2_1/n$ space group is #10, $a^-a^-b^+$ [25–27]. In the title compounds, the Li^+ and Os^{5+} cations lie on the octahedral sites while the Ln^{3+} cations occupy the A site in an 8-fold coordination environment.

There exist examples of Os(V) stabilized in the B site of the double perovskite structure type. The Os–O bond distances in Ln_2LiOsO_6 (Ln = La, Pr, Nd, Sm) range from 1.953 to 1.967 Å and are consistent with the values observed in other Os(V) oxides with this structure type [2]. The Li–O distances in Ln_2LiOsO_6 (Ln = La, Pr, Nd, Sm) range from 2.044 to 2.158 Å and are typical for Li^+ in an octahedral environment within the monoclinic double perovskite structure type [5].

The distortion from the ideal cubic double perovskite structure for the compositions discussed in this paper is a result of the tilting of the LiO_6 and OsO_6 octahedra, while maintaining their corner-sharing connectivity. This is commonly observed for compositions that include an A cation that is too small to fill the 12-fold coordination site and results in a reduced 8-fold coordination environment for the A cation in the monoclinic structure. The smaller the A cation, the greater the degree of distortion of the Li–O–Os bond angles away from the ideal 180°. In the case of the title compounds, Ln_2LiOsO_6 (Ln = La, Pr, Nd, Sm), as the size of the A cation decreases the tilting of the octahedra increases while the Li–O–Os bond angles deviate more from 180°, Table 3. This feature of rotated octahedra, common among all $P2_1/n$ ordered double perovskites, requires that the BO_6 and $B'O_6$ octahedra have different tilt angles as a result of the differences in the size and distortion of each of the two polyhedra. These tilt angles can be calculated using a set of equations derived by Groen

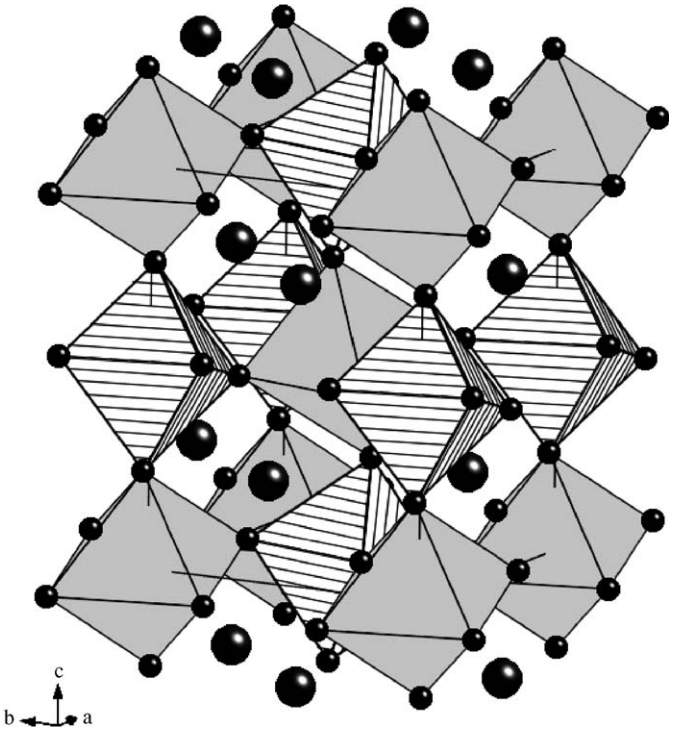

Fig. 2. Approximate (110) view of the crystal structure of Pr_2LiOsO_6 (representative of the series Ln_2LiOsO_6 (Ln = La, Pr, Nd, Sm) consisting of OsO_6 octahedra (striped) and LiO_6 octahedra (gray). Praseodymium cations are shown as large black spheres and oxygen atoms as small black spheres.

et al. from the unit cell parameters and atomic coordinates [28]. An alternative method of determining the tilt angles for the BO_6 and $B'O_6$ octahedra is based on the atomic coordinates and the average B–O bond distances and can be generated from the Tilting Using Backward Equations Relationship Software (TUBERS) program associated with the Structure Prediction Diagnostic Software (SPuDS) [29]. As the size of the Ln^{3+} cation decreases, the BO_6 and $B'O_6$ octahedra must tilt more to accommodate, and this trend is clearly observed from the tilt angles calculated using the equations by Groen that are listed in Table 4.

Based on the Goldschmidt [30] tolerance factor for perovskites of the composition $A_2BB'O_6$, one would expect that Ln^{3+} cations smaller than Sm^{3+} may be stabilized in the A site. The Goldschmidt tolerance factors are 0.93, 0.92, 0.91, and 0.90 for Ln_2LiOsO_6 (Ln = La, Pr, Nd, Sm), respectively. The smallest tolerance factors for similar compounds in this structure type have been shown to be near or around 0.86 [31]. However, no compositions of Ln_2LiOsO_6 could be prepared with a lanthanide smaller than samarium using the present synthetic technique. This peculiarity may be due to the air and water sensitivity commonly observed in lithium containing crystals, or due to unfavorable reaction conditions.

Table 4
Octahedral tilting in Ln_2LiOsO_6 (Ln = La, Pr, Nd, Sm) calculated from single-crystal data using equations of Groen et al. or TUBERS [28,29]

	w[001] tilt (deg)	j[110] tilt (deg)
La_2LiOsO_6		
LiO_6	9.2	12.5
OsO_6	9.8	13.3
Pr_2LiOsO_6		
LiO_6	11.2	14.1
OsO_6	12.3	14.8
Nd_2LiOsO_6		
LiO_6	11.6	14.4
OsO_6	12.8	15.1
$SmLiOsO_6$		
LiO_6	12.2	15.6
OsO_6	13.6	16.3

3.2. Magnetic properties

3.2.1. La_2LiOsO_6

The temperature dependence of the susceptibility for La_2LiOsO_6 in an applied field of 10 kG is shown in Fig. 3a. Fitting the high-temperature susceptibility ($100 < T < 300$) to the Curie–Weiss law results in values of $\mu_{eff} = 3.44\,\mu_B$, $C = 1.50$ emu/mol K, and $\theta = -168$ K. This value is lower than the expected moment of $3.87\,\mu_B$ for Os(V) d^3 due to spin–orbit coupling but is in good agreement with the analogous Ln_2NaOsO_6 effective moment of $3.26\,\mu_B$ [2]. The large negative Weiss temperature (−168 K) is indicative of strong antiferromagnetic interactions, and the plot does show a downturn in the susceptibility corresponding to an antiferromagnetic transition ($T_N = 39$ K). These values are also consistent those reported for a powder sample of La_2LiOsO_6 by Hayashi [22].

3.2.2. Pr_2LiOsO_6

The temperature dependence of the susceptibility for Pr_2LiOsO_6 in an applied field of 10 kG is shown in Fig. 3b. Fitting the high-temperature susceptibility ($100 < T < 300$) to the Curie–Weiss law results in values of $\mu_{eff} = 6.10\,\mu_B$, $C = 4.68$ emu/mol K, and $\theta = -38$ K. This moment is lower than the theoretical value of $6.37\,\mu_B$, but is in agreement if the moment of Os(V) is taken to be $3.44\,\mu_B$ obtained from La_2LiOsO_6, yielding a theoretical value of $6.12\,\mu_B$. The effective moment is also consistent with the moment in the analogous Pr_2NaOsO_6 ($6.28\,\mu_B$). However, Pr_2LiOsO_6 exhibits an antiferromagnetic transition at low temperatures ($T_N = 35$ K) and shows no indication of ferromagnetism or canted antiferromagnetism as observed in Pr_2NaOsO_6 [2].

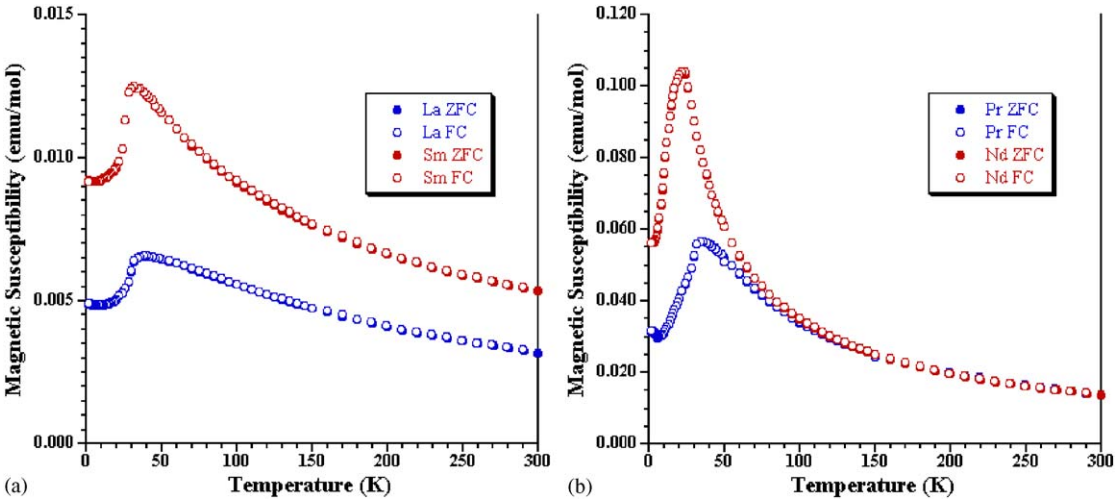

Fig. 3. Temperature dependence of the susceptibility of (a) Ln_2LiOsO_6 (Ln = La, Sm) and (b) Ln_2LiOsO_6 (Ln = Pr, Nd) in an applied field of 10 kG.

3.2.3. Nd_2LiOsO_6

The temperature dependence of the susceptibility for Nd_2LiOsO_6 in an applied field of 10 kG is shown in Fig. 3b. Fitting the high-temperature susceptibility ($100 < T < 300$) to the Curie–Weiss law results in values of $\mu_{eff} = 6.00\,\mu_B$, $C = 4.53$ emu/mol K, and $\theta = -29$ K, which agrees reasonably well with the theoretical value ($6.42\,\mu_B$). The calculated moment for Nd_2LiOsO_6, as in Pr_2LiOsO_6, agrees better with a theoretical moment of $6.17\,\mu_B$ using the moment for Os(V) obtained from La_2LiOsO_6. Interestingly, Nd_2NaOsO_6 [2] and Nd_2LiOsO_6 have the same effective moment, yet no indication of ferromagnetism or canted antiferromagnetism is observed in the lithium analog. The plot does show an antiferromagnetic transition at low temperature ($T_N = 23$ K).

3.2.4. Sm_2LiOsO_6

The temperature dependence of the susceptibility for Sm_2LiOsO_6 in an applied field of 10 kG is shown in Fig. 3a. The plot shows an antiferromagnetic transition at low temperature ($T_N = 32$ K). The high-temperature susceptibility ($100 < T < 300$) can be satisfactorily fit to the Curie–Weiss law which results in values of $\mu_{eff} = 4.52\,\mu_B$, $C = 2.56$ emu/mol K, and $\theta = -179$ K. Assuming the moment from Os(V) is $3.44\,\mu_B$, from La_2LiOsO_6, this yields an effective moment of $2.07\,\mu_B$ for Sm^{3+}.

It is interesting to note that several series of compounds, where both the lithium and sodium analogs were prepared, exhibit magnetic properties that differ noticeably. For example, in the 6H-perovskites $Ba_3MRu_2O_9$ (M = Li, Na), the sodium analog undergoes a significant susceptibility drop at 210 K concomitant with a structure transition (hexagonal to orthorhombic), while the lithium compound experiences only a slight drop in susceptibility at about 140 K with no change in crystal structure [32]. In Ba_2MOsO_6 (M = Li, Na) the lithium analog orders antiferromagnetically at 8 K while the susceptibility data of the sodium compound exhibits a field dependence below 8 K and is considered a canted antiferromagnet [18]. As briefly mentioned above, in the case of three of the four title compounds, Ln_2LiOsO_6 (Ln = La, Pr, Nd), we have previously reported on the structure and magnetic properties of the sodium analogs. While each of the lithium compounds, as reported herein, undergoes an antiferromagnetic transition between 23 and 40 K, the sodium analogs show very complex magnetic behavior and indications of ferromagnetism at temperatures below 25 K [2].

At least two factors are impacting the magnetic behavior—the lattice parameters, which determine the Os–Os and Os–Ln (in case of the magnetic rare earths) separations, and the octahedral tilt angles, which determine the Os–O–M (M = Li, Na) angle. Shorter Os–Os and Os–Ln distances will increase magnetic coupling, while increased octahedral tilt angles will reduce favorable orbital overlap for antiferromagnetic interactions. The lithium series has lattice parameters that are significantly smaller than those of the sodium series, in fact the cell volumes for the lithium series are about 9% smaller than those of the analogous sodium containing compounds, thus favoring Os–Os and Os–Ln coupling with decreased Os–Os and Os–Ln separations. With respect to the OsO_6 tilt angles, the most pronounced difference between the Li and Na series is found in the j(110) tilts, Fig. 4. The largest j(110) tilt for the Li series is 16.3° (Sm_2LiOsO_6) which is significantly smaller than the equivalent tilt for La_2NaOsO_6 (19.1°). While these factors undoubtedly all play a role in the magnetic behavior of these phases, it is not possible at this time to quantify the degree to which they contribute to the overall observed magnetism.

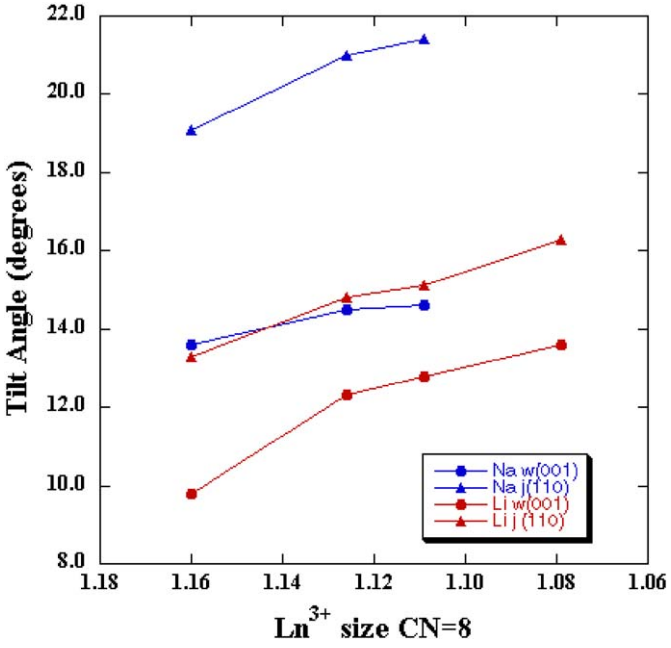

Fig. 4. OsO_6 tilt angles as a function of Ln^{3+} size (CN = 8) for the two series of double perovskites, Ln_2MOsO_6 (Ln = La, Pr, Nd, Sm, M = Li, Na).

4. Conclusions

Osmium double perovskite oxides, Ln_2LiOsO_6 (Ln = La, Pr, Nd, Sm), have been prepared as single crystals from acidic molten hydroxide. All four oxides crystallize in the monoclinic space group $P2_1/n$ (Glazer tilt system #10, $a^-a^-b^+$), forming a 1:1 ordered rock salt lattice of Li^+ and Os^{5+} cations. Magnetic susceptibility measurements show that these compounds are antiferromagnetic at low temperature with ordering temperatures of 39, 35, 23, and 32 K for Ln_2LiOsO_6 (Ln = La, Pr, Nd, Sm), respectively.

5. Supplementary material

Further details of the crystal structure investigations can be obtained from the Fachinformationszentrum Karlsruhe, 76344 Eggenstein-Leopoldshafen, Germany;

fax: +49 7247 808 666; *E-mail address*: crystdata@fizkarlsruhe.de on quoting the depository numbers CSD-416496 for Sm_2LiOsO_6, CSD-416197 for Pr_2LiOsO_6, CSD-416498 for Nd_2LiOsO_6, and CSD-416199 for La_2LiOsO_6.

Acknowledgments

Financial support from the Department of Energy through Grant DE-FG02-04ER46122 and the National Science Foundation through Grant DMR:0450103 is gratefully acknowledged.

References

[1] M.J. Davis, S.J. Mugavero III, K.I. Glab, M.D. Smith, H.-C. zur Loye, Solid State Sci. 5 (2004) 413.
[2] W.R. Gemmill, M.D. Smith, R. Prozorov, H.-C. zur Loye, Inorg. Chem. 44 (2005) 2639.
[3] W.R. Gemmill, M.D. Smith, H.-C. zur Loye, J. Solid State Chem. 177 (2004) 3560.
[4] S.J. Mugavero III, I.V. Puzdrjakova, M.D. Smith, H.-C. zur Loye, Acta Crystallogr. E 61 (2005) i3.
[5] S.J. Mugavero III, M.D. Smith, H.-C. zur Loye, J. Solid State Chem. 178 (2004) 200.
[6] H. Flood, T. Forland, Acta Chem. Scand. 1 (1947) 592.
[7] H.Z. Lux, Z. Elektrochem. 45 (1939) 303.
[8] S.W. Keller, V.A. Carlson, D. Sanford, F. Stenzer, A.M. Stacy, G.H. Kwei, M. Alario-Franco, J. Am. Chem. Soc. 116 (1994) 8070.
[9] J.L. Luce, A.M. Stacy, Chem. Mater. 9 (1997) 1508.
[10] J. Goret, Bull. Soc. Chim. (1964) 1074.
[11] S. Yonezawa, Y. Muraoka, Y. Matsushita, Z. Hiroi, J. Phys.: Condens. Matter 16 (2004) L9.
[12] S. Yonezawa, Y. Muraoka, Y. Matsushita, Z. Hiroi, J. Phys. Soc. Jpn. 74 (2004) 819.
[13] J. Reading, M.T. Weller, J. Mater. Chem. 11 (2001) 2373.
[14] A.W. Sleight, J.L. Gillson, J.F. Weiher, W. Bindloss, Solid State Commun. 14 (1974) 357.
[15] Y. Hinatsu, M. Wakeshima, Solid State Commun. 136 (2005) 499.
[16] C. Muhle, A. Karpov, A. Verhoeven, M. Jansen, Z. Anorg. Allg. Chem. 631 (2005) 2321.
[17] K.M. Mogare, W. Klein, M. Jansen, Z. Anorg. Allg. Chem. 631 (2005) 469.
[18] K.E. Stitzer, M.D. Smith, H.-C. zur Loye, Solid State Sci. 4 (2002) 311.
[19] K.E. Stitzer, A.E. Abed, M.D. Smith, M.J. Davis, S.J. Kim, J. Darriet, H.-C. zur Loye, Inorg. Chem. 42 (2003) 947.
[20] W.R. Gemmill, M.D. Smith, Y.A. Mozharivsky, G.J. Miller, H.-C. zur Loye, Inorg. Chem. 44 (2005) 7047.
[21] R. Macquart, S.J. Kim, W.R. Gemmill, J.K. Stalick, Y. Lee, T. Vogt, H.-C. zur Loye, Inorg. Chem. 44 (2005) 9676.
[22] K. Hayashi, G. Demazeau, M. Pouchard, C. R. Seances Acad. Sci. 292 (Serie 2) (1981) 1433.
[23] SMART Version 5.630, SAINT+ Version 6.45 and SADABS Version 2.10. Bruker Analytical X-ray Systems, Inc., Madison, WI, USA, 2003.
[24] G.M. Sheldrick, SHELXTL Version 6.14, Bruker Analytical X-ray Systems, Inc., Madison, WI, USA, 2000.
[25] A.M. Glazer, Acta Crystallogr. B 28 (1972) 3384.
[26] P.M. Woodward, Acta Crystallogr. B 53 (1997) 32.
[27] P.M. Woodward, Acta Crystallogr. B 53 (1997) 44.
[28] W.A. Groen, F.P.F. van Berkel, D.J.W. IJdo, Acta Crystallogr. C 42 (1986) 1472.
[29] M.W. Lufaso, P.M. Woodward, Acta Crystallogr. B 57 (2001) 725.
[30] V.M. Goldschmidt, Geochemische Verteilungsgesetze der Elementer V11, Naturvidenskaplig Klasse, Oslo, 1926.
[31] R.M. Mitchell, Perovskites: Modern and Ancient, Almaz Press, Thunder Bay, 2002.
[32] K.E. Stitzer, M.D. Smith, W.R. Gemmill, H.-C. zur Loye, J. Am. Chem. Soc. 124 (2002) 13877.